DOI: 10.1002/ejic.200600268

Synthesis, Characterization, and Luminescence Properties of Eu^{3+} 3-Phenyl-4-(4-toluoyl)-5-isoxazolonate Based Organic-Inorganic Hybrids

Patricia P. Lima,[a,b] Severino A. Junior,[a] Oscar L. Malta,[a] Luis D. Carlos,[b] Rute A. Sá Ferreira,[b] Rani Pavithran,[c] and M. L. P. Reddy*[c]

Keywords: Organic-inorganic hybrids / Eu^{3+} / Heterocyclic β-diketonates / Synthesis / Characterization / Luminescence

Organic-inorganic hybrids incorporating $Eu(TPI)_3{\cdot}3H_2O$ or $Eu(TPI)_3{\cdot}2TOPO$ [where TPI and TOPO stand for 3-phenyl-4-(4-toluoyl)-5-isoxazolone and tri-*n*-octylphosphane oxide, respectively] were synthesized either by acetic acid solvolysis or a conventional hydrolysis sol-gel route. The host framework of these materials, named as di-ureasil, consists of a siliceous skeleton grafted, through urea cross-linkages, to both ends of poly(ethylene oxide) chains. The resulting Eu^{3+}-based di-ureasils were characterized by X-ray diffraction and Fourier transform mid-IR, ^{29}Si and ^{13}C NMR, and photoluminescence spectroscopy. The room-temperature photoluminescence (PL) spectra of the Eu^{3+}-based di-ureasils display the typical Eu^{3+} red emission, assigned to transitions between the first excited state ($^5D_0$) and the ground multiplet ($^7F_{0-4}$). Enhanced $^5D_0$ quantum efficiency (η = 13 % vs. 32 %) and a longer lifetime (τ = 0.30 vs. 0.42 ms) was noticed for the hybrid incorporating the $Eu(TPI)_3{\cdot}3H_2O$ complex, compared with the undoped complex. The enhancement is explained by the coordination ability of the organic counter part of the host structure, which is strong enough to displace the water molecules of the $Eu(TPI)_3{\cdot}3H_2O$ complex from the Eu^{3+} neighborhood in the hybrids. On the other hand, a decrease in the $^5D_0$ quantum efficiency (η = 76 % vs. 61 %) and lifetime (τ = 0.98 vs. 0.75 ms) was noticed for the hybrid incorporating the $Eu(TPI)_3{\cdot}2TOPO$ complex, relative to the undoped complex, probably because of an increase in the nonradiative transition probability.

Introduction

Lanthanide complexes with organic ligands are of great interest for a wide range of photonic applications, such as tuneable lasers, optical fibres for telecommunications, components of emitting layers in multilayer organic light-emitting diodes (OLEDs), and light conversion molecular devices (LCMDs).[1–5] The β-diketone ligand is one of the most important "antenna" from which the energy can be effectively transferred to lanthanide ions for high harvest emissions.[4] Despite lanthanide β-diketonate complexes being characterized by a highly efficient light emission under UV excitation they have not been employed so far as tuneable solid-state lasers or phosphor devices essentially because of their low thermal and photochemical stability and poor mechanical properties.[6] Furthermore, lanthanide β-diketonate chelates are usually isolated as hydrates in which two or three water molecules are included in the first coordination sphere of the central metal ion, quenching the emission from the activation of nonradiative decay paths.[4,7–8]

One of the strategies adopted in recent years to simultaneously improve the thermal stability, mechanical properties, and light-emission properties of lanthanide β-diketonate complexes is to incorporate these complexes into sol-gel-derived organic-inorganic hybrids.[9–13] The main interest of the organic-inorganic hybrid concept basically derives from the possibility of tailoring the properties of novel multifunctional advanced materials through the combination, at the nanosize level, of the organic and inorganic components in one single material.[14,15] Among the sol-gel-derived structures proposed so far, a family of interesting lanthanide-based hybrid compounds have been reported.[16] The host matrix, termed as di-ureasil, comprises poly(ethylene oxide) (PEO) chains of variable length grafted to both ends to a siliceous backbone through urea cross linkages. These xerogels, which are easily produced as thin, elastomeric and highly transparent monoliths, may withstand a large amount of guest dopants. When doped with trivalent lanthanide ions like Nd^{3+}, Eu^{3+}, and Tb^{3+} the di-ureasils display remarkable emission properties. Besides a broad long-lived emission covering the whole visible range of the electromagnetic spectrum, the di-ureasils exhibit the typical intra-4f narrow line emission in the green (Tb^{3+}),[17] red (Eu^{3+}),[18–20] and even in the near infrared (Nd^{3+}) region,[21] thus opening new prospects for their applications.

[a] Departamento de Quimica Fundamental – UFPE, 50670-901 Recife, PE, Brazil
[b] Departamento de Fisica, CICECO, Universidade Aveiro, 3810-193 Aveiro, Portugal
[c] Chemical Sciences and Technology Division, Regional Research Laboratory (CSIR), Thiruvananthapuram 695019, India
E-mail: mlpreddy@yahoo.co.uk

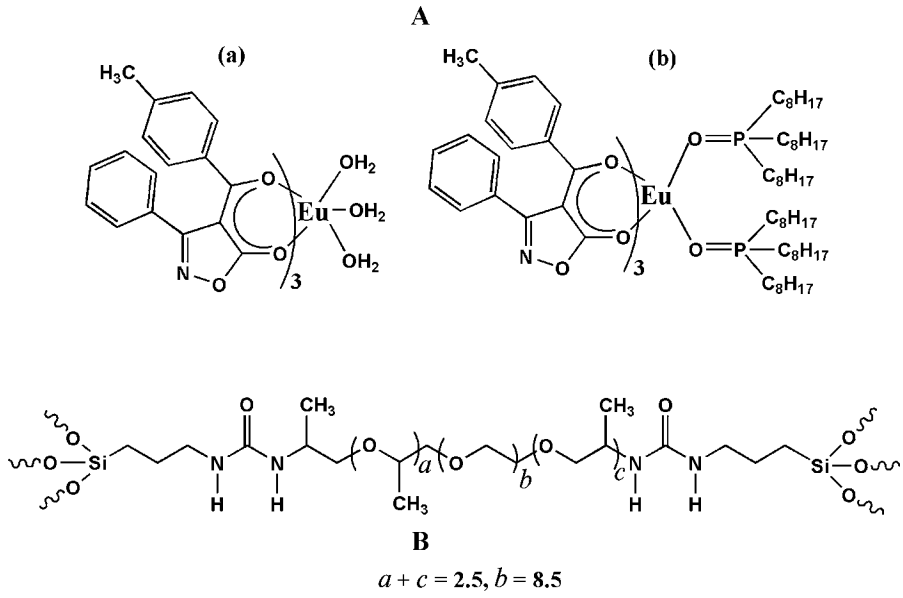

Figure 1. A: Chemical structure of (a) $Eu(TPI)_3{\cdot}3H_2O$ (**1**) and (b) $Eu(TPI)_3{\cdot}2TOPO$ (**2**); B: d-U(600) di-ureasil hybrid.

A significant part of the research strategy in the field involves the encapsulation of lanthanide organic complexes with β-diketonates, aromatic carboxylic acids and heterocyclic ligands in sol-gel-derived matrices. These complexes can be embedded in the matrix by using the ligands covalently grafted to the framework or by anchoring the lanthanide ion to specific functional groups of the hybrid matrix. Recently, Eu^{3+} β-diketonate complexes have been successfully incorporated into organic-inorganic hybrids and their photophysical properties have been investigated.[9–11] Nevertheless, the incorporation of heterocyclic β-diketonate complexes, namely Eu^{3+} 4-acyl-3-phenyl-5-isoxazolonate complexes, into organic-inorganic hybrids has not been attempted to date.

In this paper, heterocyclic β-diketone Eu^{3+} complexes with the molecular formulae $Eu(TPI)_3{\cdot}3H_2O$ and $Eu(TPI)_3{\cdot}2TOPO$ [where TPI = 3-phenyl-4-(4-toluoyl)-5-isoxazolone and TOPO = tri-*n*-octylphosphane oxide], recently introduced as light conversion molecular devices by Reddy et al.,[22] were incorporated into di-ureasil organic-inorganic hybrids (Figure 1) by conventional hydrolysis and acetic acid solvolysis. The photoluminescence (in excitation and emission modes), the $^5D_0$ quantum efficiency, and lifetime of the di-ureasil hybrids were investigated and compared with those of the precursor complexes.

Results and Discussion

The synthesis procedures and characterization of the complexes $Eu(TPI)_3{\cdot}3H_2O$ (**1**) and $Eu(TPI)_3{\cdot}2TOPO$ (**2**) (Figure 1A) are detailed in our earlier publication.[22] The complexes **1** and **2** were incorporated into the di-ureasil host by acetic acid solvolysis according to the procedure described elsewhere.[10] Complex **2** was also incorporated into di-ureasil by a conventional hydrolysis sol-gel route.[10] Figure 1B illustrates the structure of the undoped hybrid matrix.

Powder X-ray Diffraction (XRD)

The X-ray diffraction patterns of d-U(600)-**1**-AA [$Eu(TPI)_3{\cdot}3H_2O$ (**1**) incorporated into the d-U(600) di-ureasil by acetic acid (AA) solvolysis], d-U(600)-**2**-AA [$Eu(TPI)_3{\cdot}2TOPO$ (**2**) incorporated into the d-U(600) di-ureasil by acetic acid (AA) solvolysis], and d-U(600)-**2** [$Eu(TPI)_3{\cdot}2TOPO$ (**2**) incorporated into the d-U(600) di-ureasil by conventional hydrolysis] are shown in Figure 2. The patterns display a main peak centered at ca. 21.0–21.7° associated with ordering within the siloxane domains. The second-order peak appears as a broad weak hump around 38–46°. The structural unit distance, calculated using the Bragg law, is approximately 4.07–4.21 Å. These results are similar to those reported for carboxylic acid solvolysis derived undoped hybrids.[14] These data reveal that the Eu^{3+}-based hy-

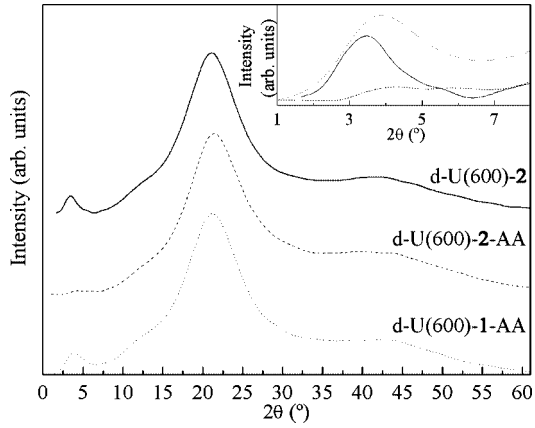

Figure 2. XRD patterns of the Eu^{3+}-based di-ureasil hybrids.

brids are highly amorphous. The peak appearing at lower angles in the XRD patterns, at ca. 3.5 and 5.2° (inset of Figure 1), has been assigned to interparticle scattering interference between siliceous domains[23] located at the ends of the polymer chain and spatially correlated at a mean distance of 25 ± 1 Å, for d-U(600)-**1**-AA, 28 ± 1 Å, for d-U(600)-**2**, and 19 ± 1 Å, for d-U(600)-**2**-AA. The different values calculated for the hybrids incorporating complex **2** indicate that the synthesis methods induce significant differences in the hybrid structure.

Fourier-Transform Infrared Spectroscopy (FT-IR)

The FT-IR spectra of d-U(600)-**1**-AA, d-U(600)-**2**-AA, and d-U(600)-**2** are shown in Figure 3. The shoulder at ca. 920 cm^{-1} provides evidence that in the di-ureasils the PEO chains attain complete disorder. Compared with the undoped di-ureasil,[24] the intensity of the shoulder shows a very slight decrease, indicating a very weak interaction between the polymer and the complex.[10] The bands at 1324 cm^{-1} are characteristic of the amorphous state.[10] The 1354 cm^{-1} bands, ascribed to the CH_2 wagging vibrations, are clearly seen in the spectra. It is known that the νCO mode of PEO is an excellent tool to probe the changes that the polymer chains of the hybrids undergo upon incorporation of the guest compounds. The fact that peaks at about 1110 cm^{-1}, characteristic of noncoordinated oxyethylene moieties,[24] are almost unchanged in the spectra of the Eu^{3+}-based di-ureasils suggests that the PEO chains of the host materials persist in an uncomplexed state.

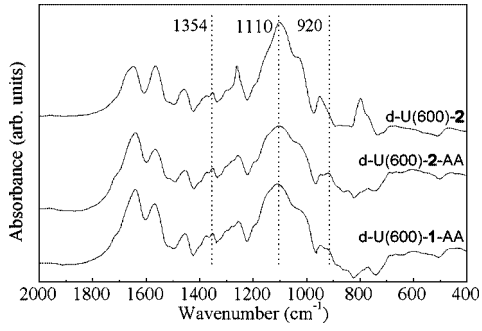

Figure 3. FTIR spectra of the Eu^{3+}-based di-ureasil hybrids.

In order to study in detail the vibrations of the urea groups, spectral deconvolutions to the so-called "amide I" (1800–1600 cm^{-1}) and "amide II" (1600–1500 cm^{-1}) regions were carried out using Gaussian band shapes, as reported elsewhere.[14,24] Three components were isolated for the "amide I" band at 1700, 1672, and 1647 cm^{-1}. According to the literature,[19,24] the former two components are ascribed to the vibrations of urea–polyether hydrogen-bonded structures, whereas the last one is ascribed to the strong self-associated hydrogen-bonded urea–urea associations. For the Eu^{3+}-doped di-ureasils, besides the three mentioned peaks, a new peak appears at 1619–1625 cm^{-1}, indicating an effective interaction between the Eu^{3+} ions and the carbonyl oxygen atoms of the urea cross-links. While for the hybrids incorporating complex **1** this result suggests the probable substitution of the water molecules in the Eu^{3+} coordination sphere, for those with complex **2** an interaction between the Eu^{3+} ions and the urea cross-links through the carbonyl groups should occur. In addition, the absence of an individual band at ca. 1750 cm^{-1} in all the spectra indicates that neither C=O nor N–H groups from urea cross-linkages are left free in the hybrid materials.[10] The "amide II" mode is a mixed contribution of the N–H in-plane bending, C–N stretching, and C–C stretching vibrations, peaking, for all the samples, at ca. 1565 cm^{-1}.

NMR Spectra

The ^{29}Si MAS NMR spectra of d-U(600)-**1**-AA and d-U(600)-**2**-AA exhibit broad signals characteristic of T_1, T_2, and T_3 units (Figure 4). These sites are labeled using the conventional T_n notation, where n (n = 1, 2, 3) is the number of Si-bridging oxygen atoms. The absence of T_0 indicates that, although the polycondensations are not, in most cases, complete, no precursor is left unreacted. The T_2 and T_3 environments (at $\delta \approx -58$ and –66 ppm, respectively) are clearly dominant, showing the presence of two main types of local structures: $(SiO)_2Si(CH_2)_3OH$ and $(SiO)_3Si(CH_2)_3$. The very weak shoulder displayed in these hybrids at $\delta \approx 51.5$ and 53.1 ppm, for d-U(600)-**1**-AA and d-U(600)-**2**-AA, respectively, is ascribed to T_1 sites. The condensation degree c (Table 1), was calculated using the expression $c = 1/3(\%T_1 + 2\%T_2 + 3\%T_3)$. Compared with the undoped sample[14] the condensation degree decreases, suggesting that there are some interactions between the complex and the matrix (urea cross-links) and that the relatively larger molecular size for the complex sterically prevents the polycondensation process and results in the lower condensation degree.

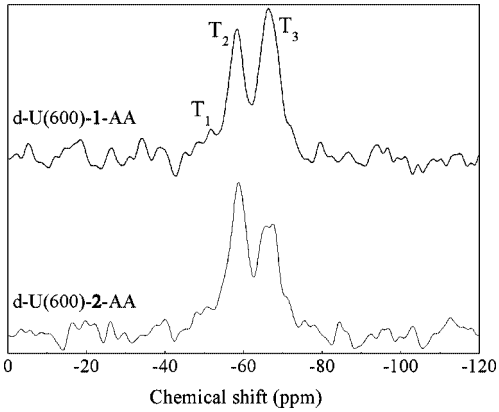

Figure 4. ^{29} Si MAS NMR spectra of the Eu^{3+}-based di-ureasil hybrids prepared by solvolysis.

The ^{13}C CP MAS NMR spectra of d-U(600)-**1**-AA and d-U(600)-**2**-AA display a peak at δ = 70.6 ppm, attributed to $-(OCH_2CH_2)-$, whereas the shoulder at about 75.0 ppm originates from the main-chain carbons of propylene oxide.

Table 1. ^{29}Si NMR chemical shifts (ppm), population of different T_n (n = 1, 2, 3) species (%), and degree of condensation (%), c, of d-U(600)-AA, d-U(600)-**1**-AA, and d-U(600)-**2**-AA.

Hybrids	T_1	T_2	T_3	c
d-U(600)-AA	–55.5(11)	–58.9(28)	–66.9(61)	83[10]
d-U(600)-**1**-AA	–51.5(19.3)	–58.2(25.4)	–66.5(55.3)	75.3
d-U(600)-**2**-AA	–53.1(26.8)	–58.6(27.9)	–66.6(45.3)	72.8

The peaks at ca. 46 and 24 ppm are characteristic of the $(CH_2)_3$ aliphatic chains. The signal at δ = 18.5 ppm is assigned to different CH_3 groups of the polymer chains, while the shoulder at δ = 17.4 ppm is ascribed to the ethoxy groups of the carbon atoms. The weak peak at $\delta \approx 159$ ppm is associated with the C=O groups of the urea linkages,[25,26] supporting the interaction between the complex and the hybrid matrix, in agreement with the results obtained from FT-IR spectroscopy. These results are similar to those reported elsewhere.[10]

Photoluminescence

Figures 5A and B compare the room-temperature excitation spectra (monitored around the peak of the intense $^5D_0 \rightarrow {}^7F_2$ transition) of complexes **1** and **2** with those of d-U(600)-**1**-AA, d-U(600)-**2**-AA, and d-U(600)-**2**. While the spectrum of complex **1** is dominated by the intra-4f^6 lines corresponding to the $^7F_{0-1} \rightarrow {}^5D_{1-2}$ transitions, the spectrum of complex **2** displays an intense broad band, with three main components at ca. 298, 330, and 400 nm, ascribed to the ligand levels. For the latter complex the relative intensity of the intra-4f^6 lines is weaker than the absorption of the organic ligands, indicating that luminescence sensitization from the ligand excitation is more efficient than the direct intra-4f^6 absorption. Moreover, in that complex the Eu^{3+} ions are excited over a much larger wavelength range (240–440 nm) than that observed for complex **1** (310–440 nm). The spectra of the Eu^{3+}-based di-ureasils are blueshifted with respect to that of the two complexes presenting mainly a broad band (260–450 nm) peaking around 375 nm and related to the ligand levels and to the hybrid host emitting centers. This reinforces that the complex incorporation of the d-U(600) host changes the Eu^{3+} surroundings. As illustrated for complex **2** in Figure 5B, the synthesis route used to incorporate the complexes leads to slight differences in the Eu^{3+} excitation paths, as reported for analogous Eu^{3+}-based di-ureasil hybrids.[10] It is worth noting that the efficiency of the sensitized process in the hybrids is almost constant over a very broad UV/Vis spectral region (250–450 nm). Moreover, the absence of Eu^{3+} intra-4f^6 lines in the excitation spectra of the hybrids strongly suggests that the metal ions are essentially excited by an efficient sensitized process rather than by direct population of the intra-4f^6 levels (the di-ureasil host contributes to enhancing the Eu^{3+} sensitization process).

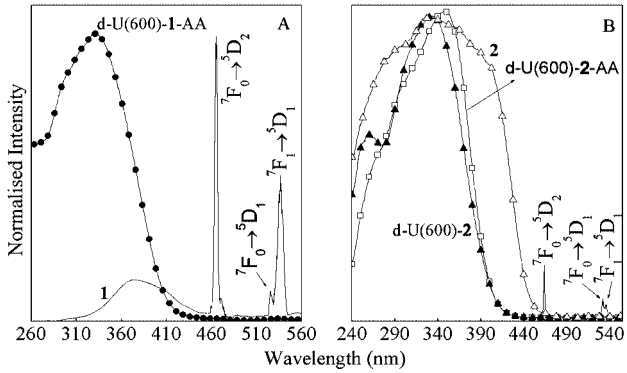

Figure 5. Room-temperature excitation spectra (monitored around 610–614 nm) of (A) complex **1** (solid line), d-U(600)-**1**-AA (solid circles) and of (B) complex **2** (open triangles), d-U(600)-**2**-AA (solid triangles), d-U(600)-**2** (open squares).

Figures 6 and 7 show the room-temperature emission spectra of the two complexes and the corresponding Eu^{3+}-based di-ureasils. The spectra display the characteristic sharp peaks of the Eu^{3+} $^5D_0 \rightarrow {}^7F_{0-4}$ transitions (575–725 nm) being dominated by the hypersensitive $^5D_0 \rightarrow {}^7F_2$ lines, which point to a highly polarizable chemical environment around the Eu^{3+} ion.[11,13] The detection of a single $^5D_0 \rightarrow {}^7F_0$ transition for all the samples investigated (Figure 6 and Figure 7B), with a typical full-width at half-maximum (fwhm) value of ca. 20 cm^{-1}, suggests the presence of a single Eu^{3+} chemical environment. The detection of that line, the local-field splitting of the $^7F_{1,2}$ levels in the 3 and 4 Stark components (Figure 6, Figure 7C and D) and the higher intensity of the $^5D_0 \rightarrow {}^7F_2$ transition indicate that the Eu^{3+} local coordination site has a low symmetry without an inversion center. For the two complexes, no emission arising from the ligand triplet levels is detected, pointing to an efficient ligand-to-Eu^{3+} energy transfer. On the other hand, the emission spectra of the hybrids display a very-low-intensity band in the blue-green region, as illustrated in the inset of Figure 6 for d-U(600)-**1**-AA. This band has been as-

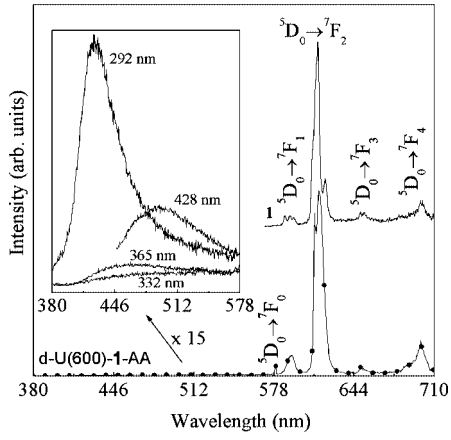

Figure 6. Room-temperature emission spectra of complex **1** (solid line) and d-U(600)-**1**-AA (solid circles), excited at 341 and 332 nm, respectively. The inset shows the magnification of the low-wavelength side of the emission spectra of d-U(600)-**1**-AA for different excitation wavelengths between 292 and 428 nm.

cribed to the hybrid host emission originated from donor–acceptor pair recombination occurring in the NH groups of the urea linkages and in the siliceous nanodomains.[27–30] The negligible intensity of this emission clearly suggests the presence of active energy transfer channels between the emitting centers of the hybrid and the Eu^{3+} ions, a claim that is in agreement with the suggested interaction between the Eu^{3+} ions and the urea cross-links through the carbonyl groups. Comparing the emission spectra of d-U(600)-**2**-AA and d-U(600)-**2** (Figure 7), changes were observed in the energy peak values, fwhm of each line, and number of Stark components, suggesting that the two different synthesis methods affect the Eu^{3+} first coordination sphere, as already noticed in the excitation spectra.

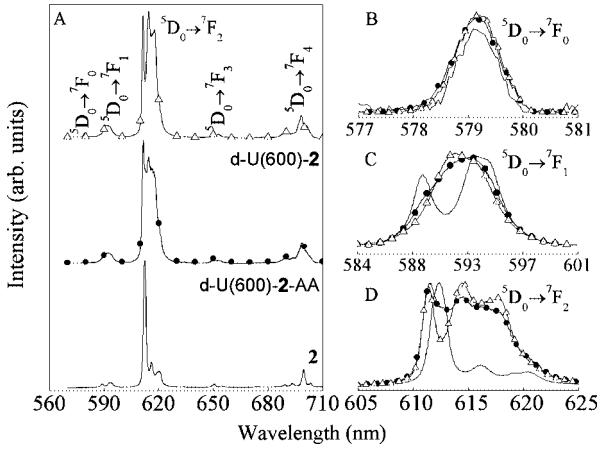

Figure 7. A: Room-temperature emission spectra of (a) complex **2**, d-U(600)-**2**-AA (solid circles) and d-U(600)-**2** (open triangles); the excitation wavelengths are 339 nm for d-U(600)-**2**, 348 nm for d-U(600)-**2**-AA and 327 nm for complex **2**. B, C, D: Details of the $^5D_0\rightarrow{}^7F_{0-2}$ transitions.

The Judd–Ofelt theory is a useful tool for analyzing f–f electronic transitions.[31] Interaction parameters of ligand fields are given by the Judd–Ofelt parameters, $\Omega\lambda$ (where λ = 2, 4, and 6). In particular, Ω_2 is more sensitive to the symmetry and sequence of ligand fields. To produce faster Eu^{3+} radiation rates, antisymmetrical Eu^{3+} complexes with larger Ω_2 parameters need to be designed. The experimental Ω_2 and Ω_4 intensity parameters were determined from the emission spectra given in Figures 6 and 7 by using the $^5D_0\rightarrow{}^7F_2$ and $^5D_0\rightarrow{}^7F_4$ electronic transitions, respectively, and by expressing the emission intensity $I_J = \hbar\omega_{J0}A_{RAD}(J)$-$N(^5D_0)$ in terms of the area under the emission curve. Here, $\hbar\omega_{J0}$ is the transition energy and N is the population of the $^5D_0$ level. The radiative emission rates, $A_{RAD}(J)$, are given by [Equation (1)],[32] where e is the electronic charge, ω the angular frequency of the transition, $\hbar$ the Planck's constant over 2π, c the velocity of light, χ the Lorentz local field correction term given by $n(n^2+2)^2/9$, where n is the refraction index, and $\langle {}^7F_J\|U^{(\lambda)}\|{}^5D_0\rangle^2$ is a squared reduced matrix element whose values are 0.0032 and 0.0023, for J = 2 and 4, respectively.[33]

$$A_{RAD} = \frac{4e^2\omega^3}{3\hbar c^3}\chi\sum_{\lambda}\Omega_\lambda\left\langle {}^7F_J\left\|U^{(\lambda)}\right\|{}^5D_0\right\rangle^2\frac{1}{2J+1} \quad (1)$$

The magnetic dipole allowed $^5D_0\rightarrow{}^7F_1$ transition was taken as the reference,[13,32] in vacuo $A_{RAD}(^5D_0\rightarrow{}^7F_1)$ = 14.65 s^{-1}.[31] An average index of refraction equal to 1.5[34] was considered leading to $A_{RAD}(^5D_0\rightarrow{}^7F_1) \approx 50\ s^{-1}$.[13] The Ω_6 parameter was not determined since the $^5D_0\rightarrow{}^7F_{5,6}$ transitions could not be experimentally detected. Table 2 lists the Ω_2 and Ω_4 intensity parameters estimated for complexes **1** and **2** and corresponding hybrids. A point to be noted is the relatively high values of the Ω_2 parameter. This might be interpreted as being a consequence of the hypersensitive behavior of the $^5D_0\rightarrow{}^7F_2$ transition.[35] The dynamic coupling mechanism is, therefore, dominant, indicating that the Eu^{3+} ion is in a highly polarizable chemical environment.

Table 2. Experimental intensity parameters (Ω_2 and Ω_4), radiative decay rates, A_{RAD}, nonradiative decay rates, A_{NRAD}, $^5D_0$ lifetimes, τ, and quantum efficiency, η, for the complex and hybrids. The parameters' errors are estimated within 5–10%.

Compounds	Ω_2 $\times10^{-20}$ [cm^2]	Ω_4 $\times10^{-20}$ [cm^2]	A_{RAD} [s^{-1}]	A_{NRAD} [s^{-1}]	τ [ms]	η [%]
Complex **1**[22]	8.1	5.8	381	2952	0.30	13
d-U(600)-**1**-AA	19.3	8.2	751	1630	0.42	32
Complex **2**[22]	20.7	6.4	773	242	0.98	76
d-U(600)-**2**	19.8	8.0	765	822	0.63	48
d-U(600)-**2**-AA	21.1	8.6	813	520	0.75	61

The $^5D_0$ lifetime values (τ) were determined by fitting the emission decay profiles to a mono-exponential function, Table 2. The shorter $^5D_0$ lifetime of complex **1**, relative to that of complex **2**, is associated with the nonradiative decay channel from the vibronic coupling with water molecules.[22] While the lifetime of the d-U(600)-**1**-AA hybrid increases around 40%, relative to that of complex **1**, the incorporation of complex **2** into the hybrid host induces a decrease of the $^5D_0$ lifetime between 24 and 36%, depending on the synthesis route. On the basis of the emission spectra and the lifetime measurements, and considering that only nonradiative and radiative processes are essentially involved in the depopulation of the $^5D_0$ state, we can estimate the emission quantum efficiency of the $^5D_0$ excited state (η) as [Equation (2)], where A_{RAD} is obtained by summing the radiative rates A_{0J} for each $^5D_0\rightarrow{}^7F_{0-4}$ transition[31] and the nonradiative rates, A_{NRAD}, are calculated from the experimental decay rates [Equation (3)].

$$\eta = \frac{A_{RAD}}{A_{RAD} + A_{NRAD}} \quad (2)$$

$$\frac{1}{\tau} = A_{RAD} + A_{NRAD} \quad (3)$$

Table 2 lists the A_{RAD}, A_{NRAD}, and η for the complexes and hybrids. The nonradiative rate of d-U(600)-**1**-AA decreases by ca. 55%, relative to that of complex **1**, causing

an enhancement in the emission quantum efficiency (η = 32%) in comparison with complex **1** (η = 13%[22]). This result is in agreement with the suggested interaction between the hybrid host and the Eu^{3+} ions through the oxygen atom of the carbonyl group, replacing water molecules present in the precursor complex. The lower $^5D_0$ quantum efficiency found for the hybrid prepared by the conventional sol-gel route, relative to that prepared by solvolysis, is mainly because of an increase in A_{NRAD}, meaning that a more efficient nonradiative channel involving the first excited triplet state exists in the former di-ureasil. These results indicate that the substitution of the water molecules in the Eu^{3+} coordination sphere of complex **1** by two TOPO molecules induces a higher $^5D_0$ emission quantum efficiency relative to the interaction with the oxygen atoms of the carbonyl groups from the d-U(600) host.

Conclusions

Di-ureasil organic-inorganic hybrids incorporating $Eu(TPI)_3{\cdot}3H_2O$ or $Eu(TPI)_3{\cdot}2TOPO$ complexes were prepared either by acetic acid solvolysis or by conventional hydrolysis. XRD and FT-IR, ^{29}Si and ^{13}C MAS NMR spectroscopic results demonstrate an effective interaction between the Eu^{3+} 3-phenyl-4-(4-toluoyl)-5-isoxazolonate complex and carbonyl groups of the urea linkages. The PL spectra of these di-ureasil organic-inorganic hybrids display the characteristic Eu^{3+} $^5D_0 \rightarrow {}^7F_{0-4}$ transitions. The broad emission typical of amine-functionalized hybrids has negligible intensity pointing to the activation of energy channels between the emitting centers of the hybrid host and the Eu^{3+} ions. The high values obtained for the experimental 4f–4f Ω_2 intensity parameters suggest that the dynamic coupling mechanism is quite operative in these compounds. The incorporation of complex **1** into the d-U(600) host enhanced the $^5D_0$ quantum efficiency and lifetime because of the coordination ability of the organic counterpart of the host structure to displace water molecules from the complex coordination sphere. A suitable choice of ligands that better sensitize the Eu^{3+} emission together with a fine control of the synthesis process definitely endorse the design of nanohybrids with better emission performance.

Experimental Section

Materials and Synthesis: The synthesis procedures of the complexes $Eu(TPI)_3{\cdot}3H_2O$ and $Eu(TPI)_3{\cdot}2TOPO$ and their characterizations are described in a recent publication.[22] The diamine α,ω-diamine-poly(oxyethylene-co-oxypropylene) with a molecular weight of about 600 a.m.u., corresponding to approximately 8.5 (OCH_2CH_2) repeat units and commercially designated as Jeffamine ED-600® (Fluka), was dried with molecular sieves (4 Å, 1.6 mm pellets, Aldrich) before use. ICPTES (3-isocyanatopropyltriethoxysilane, 95%, Fluka) and acetic acid (AA, 99.7%, Aldrich) were used without further purification. Tetrahydrofuran (THF) and absolute ethanol were dried with molecular sieves at room temperature before use. The synthesis of the di-ureasils has already been described in detail elsewhere.[14] The first stage of the synthesis involved the reaction in THF of the isocyanate group of the alkoxysilane precursor ICPTES with the terminal amine groups of the doubly functional diamine to form a urea cross-linked organic-inorganic hybrid precursor, so-called ureapropyltriethoxysilane [d-UPTES(600)]. In the second step, complexes were incorporated into the hybrid host by dissolving an appropriate amount of these complexes in ethanol and chloroform. A typical synthetic procedure was as follows.

Step 1. Synthesis of the Di-ureasil Precursor d-UPTES(600): Jeffamine ED-600® (1.0 mL, 1.75 mmol) was dissolved in dried THF (5.0 mL) in a flask in a fume hood. ICPTES (0.91 mL, 3.5 mmol) was then added to this solution whilst stirring. The molar ratio of Jeffamine ED-600/ICPTES was 1:2. The flask was sealed and the solution was stirred at room temperature under N_2 for 24 h.

Step 2. Synthesis of the Di-ureasils Incorporating $Eu(TPI)_3{\cdot}3H_2O$ and $Eu(TPI)_3{\cdot}2TOPO$ Complexes by the Conventional Sol-Gel Method or the Carboxylic Acid Solvolysis Process: The THF in the precursor solution was evaporated under vacuum, and a transparent precursor d-UPTES(600) oil was thus obtained. For the synthesis of the hybrids by the conventional sol–gel method, the $Eu(TPI)_3{\cdot}2TOPO$ complex (0.0116 mmol) was dissolved in CH_3CH_2OH (0.82 mL, 14.04 mmol), and then chloroform (0.5 mL) and HCl at pH = 2 (0.096 mL, 5.34 mmol) were added to this solution. The molar ratio of ICPTES/CH_3CH_2OH/H_2O is 1:4:3. Finally, this mixed solution was added to the precursor whilst stirring in air at room temperature. The solution was further stirred for 24 h. For the synthesis of hybrids by acetic acid solvolysis, the $Eu(TPI)_3{\cdot}3H_2O$ and $Eu(TPI)_3{\cdot}2TOPO$ complexes (0.0116 mmol) were dissolved in CH_3CH_2OH (0.82 mL, 14.04 mmol) and chloroform (0.5 mL) was added to this solution. The mixture was added to the precursor. Finally, AA (0.60 mL) was added whilst stirring under N_2 at room temperature, and the mixture was stirred for 24 h.

Experimental Techniques: Mid-IR spectra were recorded at room temperature using a MATTSON 7000 FTIR Spectrometer. The spectra were collected over the range 4000–400 cm^{-1} by averaging 64 scans at a maximum resolution of 4 cm^{-1}. The compounds were finely ground (about 2 mg), mixed with approximately 175 mg of dried potassium bromide (Merck, spectroscopic grade) and pressed into pellets. Consecutive spectra were recorded until reproducible results were obtained. X-ray diffraction patterns were recorded using a Philips X'Pert MPD Powder X-ray diffractometer system. The powders were exposed to Cu-K_α radiation (λ = 1.54 A°) at room temperature in a 2θ range (scattering angle) between 1 and 70°. The xerogel samples, analyzed as films, were not submitted to any thermal pre-treatment. ^{29}Si magic-angle spinning (MAS) and ^{13}C cross-polarization (CP) MAS NMR spectra were recorded with a Bruker Avance 400 (9.4 T) spectrometer at 79.49 and 100.62 MHz, respectively. ^{29}Si MAS NMR spectra were recorded with 2 μs (equivalent to 30°) rf pulses, a recycle delay of 60 s and at a 5.0 kHz spinning rate. ^{13}C CP/MAS NMR spectra were recorded with a 4 μs ^1H 90° pulse, 2 ms contact time, a recycle delay of 4 s, and at a spinning rate of 8 kHz. Chemical shifts are quoted in ppm from tetramethylsilane (TMS). The emission, PL, excitation, and PLE spectra and the lifetimes were measured at room temperature with a modular double grating excitation spectrofluorimeter with a TRIAX 320 emission monochromator (Fluorolog-3, Jobin Yvon-Spex), coupled to an R928 Hamamatsu photomultiplier, using the front face acquisition mode. All the photoluminescence spectra were corrected for optical and detection spectral responses.

Acknowledgments

The authors would like to acknowledge the financial support from the Defence Research and Development Organization India, the FCT (Portuguese Agency, POCTI/P/CTM/46780/02), CAPES and CNPq (Brazilian Agencies), and the RENAMI project (Brazilian Molecular and Interfaces Nanotechnology Network). The authors also wish to thank Prof. T. K. Chandrashekar, Director, Regional Research Laboratory, Trivandrum, India and Prof. C. K. Jayasanker, S. V. University, Tirupathi, India for their constant encouragement and valuable discussions.

[1] J. Kido, Y. Okamoto, *Chem. Rev.* **2002**, *102*, 2357–2368.
[2] J. C. G. Bunzli, C. Piguet, *Chem. Soc. Rev.* **2005**, *34*, 1048–1077.
[3] J. C. G. Bunzli, C. Piguet, *Chem. Rev.* **2002**, *102*, 1897–1928.
[4] G. F. de Sa, O. L. Malta, C. de Mello Donega, A. M. Simas, R. L. Longo, P. A. Santa-Cruz, E. F. da Silva Jr, *Coord. Chem. Rev.* **2000**, *196*, 165–195.
[5] D. Parker, *Coord. Chem. Rev.* **2000**, *205*, 109–130.
[6] K. Binnemans, in *Handbook on the Physics and Chemistry of Rare Earths* (Eds: A. Gschneidner Jr, J. C. G. Bunzli, V. K. Pecharsky), Elsevier, Amsterdam, **2005**, vol. 35, pp.107–272.
[7] R. Pavithran, N. S. Saleesh Kumar, S. Biju, M. L. P. Reddy, S. Alves Jr, R. O. Freire, *Inorg. Chem.* **2006**, *45*, 2184–2192.
[8] H. Xin, M. Shi, X. C. Gao, Y. Y. Huang, Z. L. Gong, D. B. Nie, H. Cao, Z. Q. Bian, F. Y. Li, C. H. Huang, *J. Phys. Chem. B* **2004**, *108*, 10796–10800.
[9] C. Molina, K. Dahmouche, Y. Messaddeq, S. J. L. Ribeiro, M. A. P. Silva, V. de Zea Bermudez, L. D. Carlos, *J. Lumin.* **2003**, *104*, 93–101.
[10] L. Fu, R. A. Sá Ferreira, N. J. O. Silva, J. A. Fernandes, P. Ribeiro-Claro, I. S. Gonçalves, V. de Zea Bermudez, L. D. Carlos, *J. Mater. Chem.* **2005**, *15*, 3117–3125.
[11] P. P. Lima, R. A. S. Ferreira, R. O. Freire, F. A. A. Paz, L. Fu, S. Alves Jr, L. D. Carlos, O. L. Malta, *ChemPhysChem* **2006**, *7*, 735–746.
[12] M. M. Silva, V. de Zea Bermudez, L. D. Carlos, A. Almeida, M. J. Smith, *J. Mater. Chem.* **1999**, *9*, 1735–1740.
[13] L. D. Carlos, Y. Messaddeq, H. M. Brito, R. A. Sá Ferreira, V. de Zea Bermudez, S. J. L. Ribeiro, *Adv. Mater.* **2000**, *12*, 594–598.
[14] L. S. Fu, R. A. Sá Ferreira, N. J. O. Silva, L. D. Carlos, V. de Zea Bermudez, J. Rocha, *Chem. Mater.* **2004**, *16*, 1507–1516.
[15] C. Sanchez, F. Ribot, B. Lebeau, *J. Mater. Chem.* **1999**, *9*, 35–44.
[16] L. D. Carlos, V. de Zea Bermudez, M. C. Duarte, M. M. Silva, C. J. Silva, M. J. Smith, M. Assuncao, L. Alcacer, in: *Physics and Chemistry of Luminescent Materials* (Eds: C. Ronda, T. Welker) VI, Electrochemical Society Proceedings, San Francisco, **1998**, vol. 97-29, p. 352.
[17] V. Bekiari, P. Lianos, P. Judeinstein, *Chem. Phys. Lett.* **1999**, *307*, 310–316.
[18] L. D. Carlos, R. A. Sá Ferreira, V. de Zea Bermudez, C. Molina, L. A. Bueno, S. J. L. Ribeiro, *Phys. Rev. B* **1999**, *60*, 10042–10053.
[19] V. de Zea Bermudez, R. A. Sá Ferreira, L. D. Carlos, C. Molina, K. Dahmouche, S. J. L. Ribeiro, *J. Phys. Chem. B* **2001**, *105*, 3378–3386.
[20] M. M. Silva, V. de Zea Bermudez, L. D. Carlos, A. Almeida, M. J. Smith, *J. Mater. Chem.* **1999**, *9*, 1735–1740.
[21] M. C. Gonçalves, N. J. O. Silva, V. de Zea Bermudez, R. A. Sá Ferreira, L. D. Carlos, K. Dahmouche, C. V. Santilli, D. Ostrovskii, I. C. Correia Vilela, A. F. Craievich, *J. Phys. Chem. B* **2005**, *109*, 20093–20104.
[22] R. Pavithran, M. L. P. Reddy, S. Alves Jr, R. O. Freire, G. B. Rocha, P. P. Lima, *Eur. J. Inorg. Chem.* **2005**, *20*, 4129–4137.
[23] K. Dahmouche, L. D. Carlos, V. De Zea Bermudez, R. A. Sá Ferreira, C. V. Santilli, A. F. Craievich, *J. Mater. Chem.* **2001**, *11*, 3249–3257.
[24] V. de Zea Bermudez, L. D. Carlos, L. Alcácer, *Chem. Mater.* **1999**, *11*, 569–580.
[25] A. C. Franville, R. Mahiou, D. Zambon, J. C. Cousseins, *Solid State Sci.* **2001**, *3*, 211–222.
[26] M. C. Gonçalves, V. de Zea Bermudez, R. A. Sá Ferreira, L. D. Carlos, D. Ostrovskii, J. Rocha, *Chem. Mater.* **2004**, *16*, 2530–2543.
[27] L. D. Carlos, V. de Zea Bermudez, R. A. Sá Ferreira, L. Marques, M. Assuncao, *Chem. Mater.* **1999**, *11*, 581–588.
[28] L. D. Carlos, R. A. Sá Ferreira, V. de Zea Bermudez, in: *Handbook of Organic-Inorganic Hybrid Materials and Nanocomposites* (Eds: H. S. Nalwa), American Scientific Publishers, Morth Lewis Way, California, **2004**, vol. 1, chapter 9, p. 353.
[29] L. D. Carlos, R. A. Sá Ferreira, V. de Zea Bermudez, S. J. L. Ribeiro, *Adv. Funct. Mater.* **2001**, *11*, 111–115.
[30] L. D. Carlos, R. A. Sá Ferreira, R. N. Pereira, M. Assunção, V. de Zea Bermudez, *J. Phys. Chem. B* **2004**, *108*, 14924–14932.
[31] M. H. V. Werts, R. T. F. Jukes, J. W. Verhoeven, *Phys. Chem. Chem. Phys.* **2002**, *4*, 1542–1548.
[32] O. L. Malta, M. A. C. dos Santos, L. C. Thompson, N. K. Ito, *J. Lumin.* **1996**, *69*, 77–84.
[33] W. T. Carnall, H. M. Crosswhite, "Energy Levels, Structure and Transition Probabilities of the Trivalent Lanthanides", in: LaF_3, Argonne National Laboratory, Illinois, **1977**.
[34] C. Molina, P. J. Moreira, R. R. Gonçalves, R. A. Sá Ferreira, Y. Messaddeq, S. J. L. Ribeiro, O. Soppera, A. P. Leite, P. V. S. Marques, V. de Zea Bermudez, L. D. Carlos, *J. Mater. Chem.* **2005**, *15*, 3937–3945.
[35] R. D. Peacock, *Struct. Bonding (Berlin)* **1975**, *22*, 83–121.

Received: March 28, 2006
Published Online: August 7, 2006

